Phase diagram of a cyclic predator-prey model with neutral-pair exchange

Nara C. Guisoni*
Instituto de Física de Líquidos y Sistemas Biológicos (IFLYSIB), Universidad Nacional de La Plata, CONICET CCT-La Plata, Calle 59-789 (1900) La Plata, Argentina

Ernesto S. Loscar†
Instituto de Investigaciones Fisicoquímicas Teóricas y Aplicadas (INIFTA), Facultad de Ciencias Exactas, Universidad Nacional de La Plata, CONICET CCT-La Plata, Sucursal 4, CC 16 (1900) La Plata, Argentina

Mauricio Girardi‡
Universidade Federal Santa Catarina, 88900-000, Araranguá, Santa Catarina, Brazil
(Received 16 April 2013; published 19 August 2013)

In this paper we obtain the phase diagram of a four-species predator-prey lattice model by using the proposed gradient method. We consider cyclic transitions between consecutive states, representing invasion or predation, and allowed the exchange between neighboring neutral pairs. By applying a gradient in the invasion rate parameter one can see, in the same simulation, the presence of two symmetric absorbing phases, composed by neutral pairs, and an active phase that includes all four species. In this sense, the study of a single-valued interface and its fluctuations give the critical point of the irreversible phase transition and the corresponding universality classes. Also, the consideration of a multivalued interface and its fluctuations bring the percolation threshold. We show that the model presents two lines of irreversible first-order phase transition between the two absorbing phases and the active phase. Depending on the value of the system parameters, these lines can converge into a triple point, which is the beginning of a first-order irreversible line between the two absorbing phases, or end in two critical points belonging to the directed percolation universality class. Standard simulations for some characteristic values of the parameters confirm the order of the transitions as determined by the gradient method. Besides, below the triple point the model presents two standard percolation lines in the active phase and above a first-order percolation transition as already found in other similar models.

DOI: 10.1103/PhysRevE.88.022133 PACS number(s): 05.70.Fh, 02.50.−r, 64.60.ah, 82.20.Wt

I. INTRODUCTION

In multispecies systems, cyclic competition represents a situation in which each species cyclically dominates some other in a such way that no one species is competitively superior to all others. The simplest and most studied lattice model of cyclic competition is composed by three species and it is equivalent to the children's game "rock-paper-scissors", where rock breaks scissors, scissors cut paper, and paper covers rock. Several versions of the cyclic three-species model have been studied in recent years in contexts related with pattern formation [1,2], population dynamics [3], theory of games [4], and others. Despite its simplicity, the rock-paper-scissors-like dynamics was found in different experimental systems such as plant communities [5], evolution of reproductive strategies [6], and in studies on bacteria diversity, both *in vitro* [7] and *in vivo* [8]. Also, several lattice Lotka-Volterra models are examples of three-species models with cyclic dynamics, such as the predator-prey or the susceptible-infected-recovered models [9,10] and the forest-fire models [11,12].

The critical behavior of three-species lattice models with cyclic competition can present an active phase, in which the different species coexist, and an absorbing phase, where only one survives, depending on the interaction rules among the involved species and the value of the control parameters. When four or more species are considered, a new ingredient appears: the mutual protection between noninteracting species (called "neutral pairs"), which leads to the formation of defensive alliances, preventing the invasion of predators. The defensive alliances allow the presence of new phases composed just by neutral pairs. In fact, the cyclic predator-prey model with several species can exhibit a very complex behavior [13,14]. For example, depending on the parity of the number of the considered species, the steady-state densities are strongly affected, leading to a parity law [15] that affects the system dynamic properties. As expected, with the inclusion of more species the cyclic models become more relevant, for example, for biological and ecological systems. This happens since real trophic networks have usually a larger diversity, represented by the number of different species [14]. However, from the theoretical point of view, the inclusion of several species in cyclic models represents an increase in fluctuations and slow domain dynamics leading to large time-consuming numerical calculations [16], making it difficult to handle.

In this paper we study a four-species cyclic predator-prey model. By changing the invasion rate of prey sites by neighboring predators, the model presents an active phase, where the four species invade each other cyclically, and two symmetric absorbing phases, composed by only two noninteracting species (neutral pairs). The transitions between the active phase and the absorbing phases were previously shown to be continuous, belonging to the directed percolation universality class [16,17]. For the case of symmetric predation,

*naraguisoni@conicet.gov.ar
†yasser.loscar@gmail.com
‡mauricio.girardi@ufsc.br

this model has also been studied with the inclusion of an exchange probability between neighboring neutral pairs [16]. In the latter case, a transition between an active phase and one of two possible symmetric absorbing phases was observed.

Our goal in this paper is to study the phase diagram for the four-species cyclic predator-prey model with neutral-pairs exchange, in which the main results and conclusions are obtained by means of the gradient method (GM) [18–20]. For some characteristic values of the parameters, the results have also been verified by using an approach with standard simulations. In the case of the GM, we apply a linear gradient in the invasion rate parameter, which allows for the presence of different phases in the same simulation. The study of a single-valued interface between the different phases gives the critical point of the irreversible phase transition. Also, the consideration of a multivalued interface brings the percolation threshold. The study of the fluctuations of the interfaces allows us to identify the corresponding universality class in the case of second-order transitions, while for the first-order transitions, we are able to study the universality class of the interface itself. In that way, the GM can help us to decide the order of an irreversible phase transition [18–20]. Therefore, we show that the present cyclic four-species model presents two lines of irreversible first-order phase transition between the two symmetric absorbing phases and the active phase. Due to the exchange between neighboring neutral pairs, the reactive window shrinks, finishing in a triple point that is the beginning of a first-order irreversible line between the two absorbing phases. On the other hand, when the exchange between neighboring neutral pairs is absent, the lines of irreversible first-order phase transition end in critical points that belong to the directed percolation universality class, as previous results [17]. For some characteristic values of the parameters, the results have also been verified by using an approach with standard simulations. We also show that below the triple point the percolation transition lies on the active phase, and has a standard percolation behavior. On the other hand, above the triple point, when the active region disappears, the model presents a first-order percolation transition.

We organized the paper as follows. In Sec. II we introduce the four-species cyclic predator-prey model. The realization of the GM for this system is shown in Sec. III. Results from the Monte Carlo simulations obtained by applying the GM are discussed in Sec. IV, and by using standard simulations in Sec. V. Finally, our conclusions are stated in Sec. VI.

II. MODEL

In the present four-species cyclic predator-prey model, each site i of a square lattice of linear size L is occupied by a single species labeled as $\sigma_i = 1,2,3,$ or 4. The system evolves through the invasion of prey sites by neighboring predators with the cyclic rule

$$1 \to 2 \to 3 \to 4 \to 1, \tag{1}$$

where the arrows mean that the left species can invade a neighboring site occupied by the right species. Since the opposite invasions are forbidden, the model presents irreversibility, which leads to the existence of absorbing states.

TABLE I. The invasion probabilities $[I(\sigma_i \to \sigma_j)]$ that a site i invades a site j, given in terms of the normalized parameter a ($0 \leqslant a \leqslant 1$). The invasion direction is given by Eq. (1).

$\sigma_i \diagdown \sigma_j$	1	2	3	4
1	0	a	0	0
2	0	0	$1-a$	0
3	0	0	0	a
4	$1-a$	0	0	0

Invasion of neighboring sites depends on the invasion parameter a and it occurs with probability $I(\sigma_i \to \sigma_j)$, as shown in Table I. The parameter a regulates the asymmetry between the odd and even species. For $a = 1/2$ all predations occur with the same probability, whereas for $a > 1/2$ ($a < 1/2$) odd (even) species are favored. The alliance between odd species or between even species leads to the formation of neutral pairs, which prevents invasion of predators. For simplicity, we call the even species as species A and the odd ones as species B.

In Fig. 1(a) the axis represents schematically the parameter a. For $a = 1/2$ we have a stationary steady state with both species present with the same probability. This active phase is labeled as active $A + B$. As the invasion parameter a increases, the species B is favored. For a large enough value of a the active state is no longer possible and the system passes to a phase composed only by species B, where no more

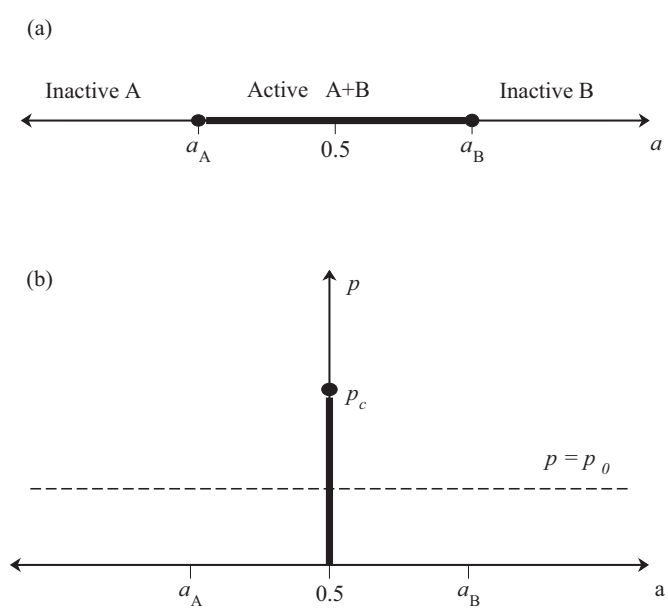

FIG. 1. System parameters a and p of the four-species cyclic predator-prey model. (a) In the line of invasion parameter ($p = 0$), there is a reactive symmetric window around $a = 1/2$ (thick line) composed by even (A) and odd species (B). The points $a = a_A$ and $a = a_B$ are critical points to an A absorbing state ($a < a_A$) and to a B absorbing state ($a > a_B$), respectively. (b) The vertical axes represents the exchange probability between neighboring neutral pairs, p. For the symmetric invasion parameter ($a = 1/2$) there is an active (thick) line, until the point $p = p_c$, where the system becomes trapped in one of the symmetrical absorbing states. The dashed line $p = p_0$ represents the points on the plane where the gradient in a is applied.

predation is possible and, therefore, constitutes an absorbing phase (inactive B). As shown in Fig. 1(a), these two phases are separated by a critical point at $a = a_B$, which has been observed as belonging to the directed percolation universality class [17]. Clearly, for decreasing a, there is a symmetrical and equivalent critical point ($a = a_A$) between the active $A + B$ phase and an inactive A phase. Therefore, one has a reactive window between a_A and a_B.

The other relevant parameter for the present model is the exchange probability p, by which neutral pairs (1 and 3, or 2 and 4) can exchange their positions. In Fig. 1(b), p is represented by the vertical axes. The model's behavior as a function of p was already studied considering symmetric interactions, that is with $a = 1/2$ [16]. For this case, the performed Monte Carlo simulations have shown the existence of a critical point $p = p_c$. In this way, the active $A + B$ phase is present for $p < p_c$, while for $p > p_c$ the system becomes irreversibly trapped in one of the two symmetric absorbing states. This spontaneous symmetry breaking has been suggested to be of first order, but the results are not conclusive [16].

We have studied here the a-p phase diagram by Monte Carlo simulations, which were carried out as follows: a square lattice with linear size L is randomly filled by the four species, with one entity per site. We choose a pair of neighboring sites (i, j) and try an invasion with probability $I(\sigma_i \to \sigma_j)$ given by Table I. Additionally, if the (i, j) pair is neutral, the exchange between i and j occurs with probability p. Due to the exchange and invasion rules, the number of entities is conserved. In one Monte Carlo step we perform L^2 trials to invade or exchange.

III. APPLYING THE GM

In the standard simulation scheme the parameters shown in Fig. 1(b) are maintained fixed, so that each point of the plane is simulated independently. Here, in accordance with the proposed gradient method (GM) [18–20], we study the model by applying a gradient in the invasion parameter a. This means that, for a square lattice of size L and a fixed value of the exchange p, the parameter a changes linearly as

$$a(j) = j/L, \tag{2}$$

where j is the column number ($1 \leqslant j \leqslant L$). This results in different invasion probabilities on different columns of the lattice. In Fig. 1(b) the dashed line indicates schematically the points of the phase space, which are being simulated with the GM in one single run for $p = p_0$. If there are transition points within the range of a, this gradient allows for the definition of interfaces between the distinct phases. Studying these interfaces one can determine the critical behavior of the transitions that occur in the system [18–20].

Figure 2(a) shows a typical snapshot obtained by the GM considering a horizontal gradient in the parameter a given by the equation (2), for $p = 0$. In the right-hand side of the sample we can see the absorbing phase composed by species 1 and 3, whereas in the left-hand side we have the absorbing phase composed by species 2 and 4. In the center of the sample it is possible to see the reactive window, where all species are present. In Fig. 2(b) we show the mapping of species 2 and 4 (1 and 3) to A (B) species for $p = 0$. Note that Figs. 2(a) and 2(b) correspond to the same snapshot. The simplest interface associated with one phase (say phase B), called the single-valued interface (SVI), is defined by the set of sites $SVI = \sigma_i$ with $i = 1, \ldots, N_{SVI}$, belonging to this phase (phase B) that is in contact with at least one site of the other phase (phase A), and is located on the rightmost side of the sample in each row i. The SVI is represented in Fig. 2(b) by dark gray circles. Since the definition of the SVI is made row by row, one has that $N_{SVI} \equiv L$. From the above definition one can obtain the location of the SVI interface (the mean value of the invasion parameter) by the equation

$$a^{SVI} = \frac{1}{N_{SVI}} \sum_{\sigma \in SVI} a(\sigma), \tag{3}$$

and the width of this interface, by

$$w^{SVI} = \sqrt{\frac{1}{N_{SVI}} \sum_{\sigma \in SVI} [a(\sigma) - a^{SVI}]^2}. \tag{4}$$

The associated critical exponent α, related to the width of the interface, is given by the scaling relation

$$w^{SVI} \propto \left(\frac{1}{L}\right)^{\alpha}, \tag{5}$$

where the exponent α is associated to the spatial correlation length critical exponent ν [19,21] by

$$\nu = \frac{1 - \alpha}{\alpha}. \tag{6}$$

Also, in order to detect the percolation transition we define a multivalued interface (MVI). For the case of B phase one first determines all B-occupied sites in contact with the massive B cluster located on the right of the sample. These sites, connected by means of nearest neighbors, are denoted as the "land". The A-occupied sites are linked through both nearest- and next-nearest-neighbor sites and form a large cluster that is termed the "sea". The sites not connected with the two large clusters of land and sea are identified as "islands" and "lakes", respectively, but they are irrelevant. In fact, the MVI interface is given by the "seashore" where land and sea are in contact. The MVI is represented in Fig. 2(b) by light gray squares. We can see that the number of sites belonging to the MVI (N_{MVI}) is greater than $N_{SVI} = L$. The same equations (3)–(6) can be considered by taking the set of points MVI instead of the set SVI, in order to determine the percolation threshold and its characteristic exponents.

Note that we have presented the construction of the SVI and MVI for the B phase. It is also possible to construct both interfaces for the A phase. However, since the model is symmetric with respect to $a = 1/2$, the results are completely equivalent. For a more detailed discussion about the definitions of SVI and MVI the reader can see the references [18–20]. All the simulation results presented in the next sections are related to the B phase.

IV. RESULTS FROM GM

In Fig. 2 we show the snapshots of typical steady states of the system as obtained with the GM for the cases of $p = 0$ [Figs. 2(a) and 2(b)], $p = 0.005$ [Figs. 2(c) and 2(d)],

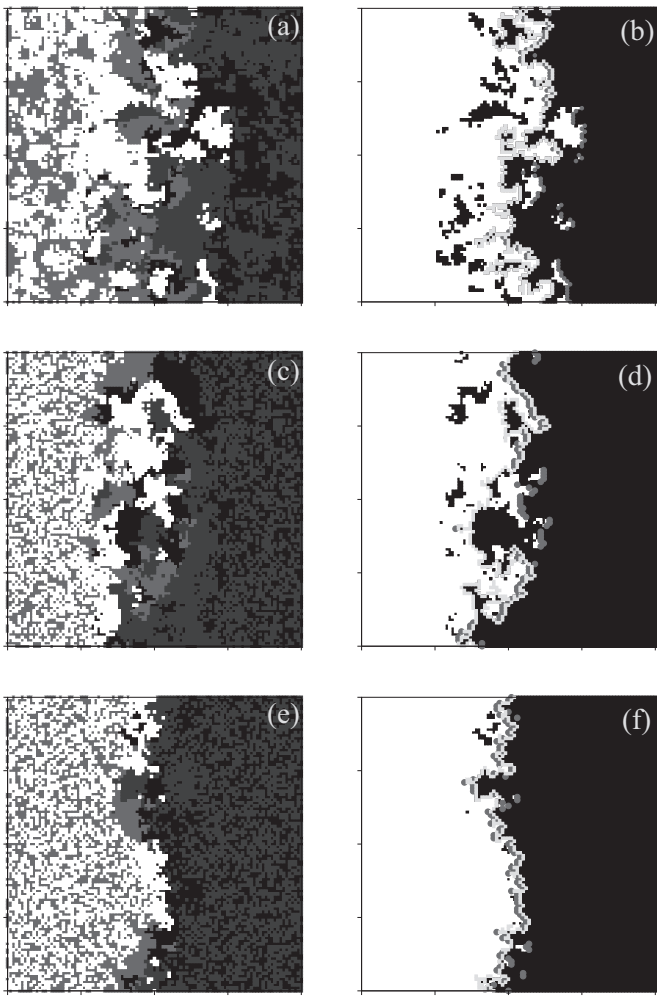

FIG. 2. Snapshots of the system with a horizontal gradient in the parameter a for a lattice of size $L = 400$. (a) and (b) correspond to the case $p = 0$, (c) and (d) correspond to $p = 0.005$, and (e) and (f) correspond to $p = 0.025$. In the left figures the species 1, 2, 3, and 4 are represented by black, light gray, dark gray, and white squares respectively. In the right figures the species 2, 4 (A) are represented in white, and 1, 3 (B) in black, while dark gray circles correspond to SVI and light gray squares belong to MVI. Note that for some rows the SVI and MVI sites coincide, mostly for higher values of p. More details are in the text.

and $p = 0.025$ [Figs. 2(e) and 2(f)]. We recall that we considered a horizontal gradient in the parameter a, as given by Eq. (2). After a relaxation of $\tau_{\text{relax}} = 10^5$ Monte Carlo steps (MCs), we have measured our stationary data during the next $\Delta t = 10^5$ MCs. These simulations correspond to the three characteristic zones as can be seen in Fig. 1(b): the horizontal axes ($p = 0$); one horizontal line below of p_c ($p = 0.005$); and one horizontal line above the p_c ($p = 0.025$). In Figs. 2(a), 2(c), and 2(e) we can observe the presence of two absorbing phases, one composed only by species 2 and 4 (A particles), on the left-hand side of the sample, and other one composed only by species 1 and 3 (B particles), on the right-hand side of the sample. The absorbing phases are separated by an active zone where the four species are present. Figures 2(b), 2(d), and 2(f) exhibit the mapping of even and odd species into A and B phases, respectively, and the SVI and

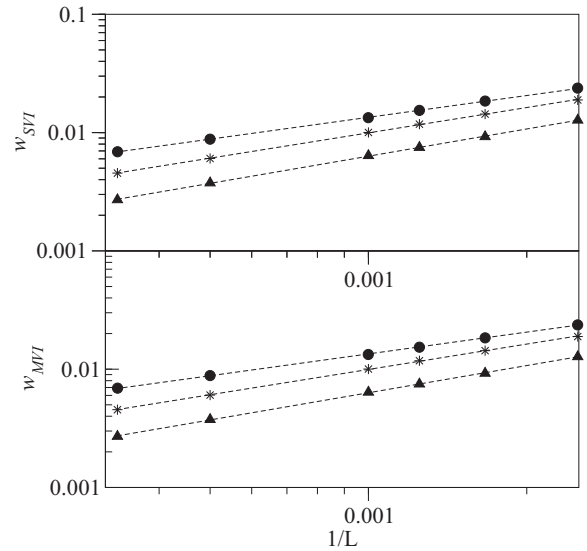

FIG. 3. The width of the SVI (w_{SVI}) and MVI (w_{MVI}) interfaces as a function of the gradient ($\Delta = 1/L$) for $p = 0$ (circles), $p = 0.005$ (stars), and $p = 0.025$ (triangles). The lines are power-law fits. From the fits (dashed lines) we obtained $\alpha_{SVI} = 0.58(36)$ for $p = 0$, $\alpha_{SVI} = 0.711(11)$ for $p = 0.005$, and $\alpha_{SVI} = 0.753(14)$ for $p = 0.025$; and $\alpha_{MVI} = 0.383(8)$ for $p = 0$, $\alpha_{MVI} = 0.438(17)$ for $p = 0.005$, and $\alpha_{MVI} = 0.748(6)$ for $p = 0.025$.

MVI interfaces corresponding to the B (right) phase. One can note that the coexistence region (composed by the four species) is observed for a smaller range of the parameter a as the value of p increases [compare Figs. 2(a), 2(c), and 2(e)]. This effect is translated on the mapping of Figs. 2(b), 2(d), and 2(f) by the smaller number of island and lakes (and consequently by a less rough MVI) for higher values of p. Also, from Fig. 2 we can see that, whereas for $p = 0.025$ MVI and SVI almost coincide, for $p = 0$ and $p = 0.005$ this is not even true.

We can gain further insights into the transitions presents in Fig. 2 by studying the SVI interface, for the case of the irreversible phase transitions (IPTs), and by studying the MVI, for the case of the percolation transition (PT). We recall that the results presented below for the IPTs and PT are related to the B phase.

A. Irreversible phase transitions

In Fig. 3(a) we exhibit the width of the SVI (w_{SVI}) as a function of the gradient $\Delta = 1/L$, for $p = 0$, $p = 0.005$, and $p = 0.025$, and using square lattices of size $L = 400, 600, 800, 1000, 2000$, and 3000. For all these values of p, the curves are well fitted by a power law which, by the use of Eq. (5), one can obtain the exponent α. Particularly, for $p = 0$, a careful analysis of α_{SVI} shows the presence of finite-size effects and the results depend slightly on the considered lattice size, as already observed in other models studied through the GM [18, 22,23]. Therefore, we have obtained $\alpha_{SVI} = 0.58(36)$ for $p = 0$, $\alpha_{SVI} = 0.711(11)$ for $p = 0.005$, and $\alpha_{SVI} = 0.753(14)$ for $p = 0.025$.

Besides, by using Eq. (6) with the value of α as obtained from Fig. 3(a), we calculate the exponent ν_{SVI}. In Fig. 4 we show the exponent ν_{SVI} for different values of p. We observe

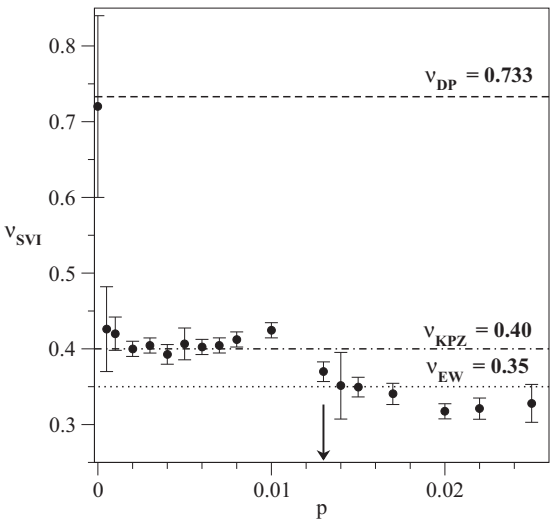

FIG. 4. The exponent ν_{SVI} as a function of the neutral exchange probability p. The long-dashed line indicates the correlation length $\nu_{DP} = 0.733$ [25] expected for the DP universality class, the dashed-point line indicates the correlation length $\nu_{KPZ} = 2/5$ [26] for the KPZ universality class, and the short-dashed line represents the correlation length $\nu_{EW} = 0.35$ [26] for the EW universality class. The arrow indicates the estimated value for the triple point ($p = P_T = 0.013 \pm 0.005$).

that for $p = 0$, when the neutral pair exchange is absent, we have $\nu_{SVI} = 0.72(12)$, which is marginally compatible with the exponent of the correlation length of the directed percolation (DP) universality class, whose value is $\nu_{DP} = 0.733(4)$ [24,25]. This result is in agreement with that already obtained by Szabò and Szolnoki [17] for $p = 0$, who have characterized this transition by means of standard simulation methods, as a second-order IPT belonging to DP class.

In contrast, for small non-null values of p we observe in Fig. 4 a sudden decrease of ν_{SVI}. This strong change reflects the underlying effect due to the exchange probability p. Note that the presence of a very little exchange $p = 0.0005$, modifies the exponent considerably (from $\nu \approx 0.7$ to about $\nu \approx 0.40$). This observation clearly suggests a change in the nature of the transition due to the condition $p \neq 0$. For higher values of p we can see from Fig. 4 that the exponent is almost unchanged until $p = P_T \sim 0.013$. For values of p higher than P_T another subtle decrease in the ν_{SVI} is observed. This new value is maintained for high values of p.

In the Fig. 4 we indicate by horizontal lines the theoretical values of the perpendicular length correlation exponents for the direct percolation (DP) universality class $\nu_{DP} = 0.733$, for the Kardar-Parisi-Zhang (KPZ) universality class $\nu_{KPZ} = 2/5$, and for the the Edwards-Wilkinson (EW) universality class $\nu_{EW} = 0.35$ [26]. We can observe, for $0.005 \leqslant p < P_T$, values of the exponent ν_{SVI} compatible with the exponent $\nu_{KPZ} = 2/5$, while for $p \geqslant P_T$ the value of ν_{SVI} is around $\nu_{EW} = 0.35$. It is worth mentioning that in the case of the EW and KPZ exponents, these exponents characterize the universality of a self-affine interface, not a true second-order transition. In fact, if there is a first-order transition present, our method generates the interface associated to this transition [18–20]. For this case, due to the absence of a diverging correlation length in the first-order transition, one has that the overall behavior is dominated by the divergence of the correlation length of the self-affine interface.

So that, the analysis of the SVI suggests that in the present cyclic predator-prey model the neutral pair exchange probability p changes the nature of the observed irreversible phase transitions: from a second-order phase transition for $p = 0$, to a first-order phase transition for $p > 0$. Also, the nature of the first-order phase transition seems to change, at some point P_T where the interface behavior changes from KPZ to EW universality class. Looking at the snapshots of Figs. 2(b) and 2(d) we can observe that the reactive window present for $p = 0$ is reduced for $p > 0$. In addition, the snapshot Fig. 2(f) for $p = 0.025 > P_T$ suggests that the reactive window is zero wide. Considering this observation, we can anticipate that the change in the critical behavior of the interface, whose universality class changes from KPZ to EW, should be related to the nature of the first-order transition, that is one between an active and an absorbing phase (with a reactive window of nonzero wide) for small non-null values of p, to another between two absorbing phases (with a zero-wide reactive window) for high values of p. This question, as well as the location of the critical points, will be seen with more detail below in Sec. IV C. Before of this, let us discuss the percolation transition through the study of the MVI.

B. Percolation transitions

Using the same set of simulations, the GM allows us to analyze the percolation transition from the behavior of the MVI. As in the case of irreversible phase transitions and the properties of the SVI, further insights into the percolation transition can be given by the exponent of the interface width w in Eq. (5). Figure 3(b) shows the width of the MVI (w_{MVI}) as a function of the gradient $\Delta = 1/L$, for $p = 0$, $p = 0.005$, and $p = 0.025$. As we can see, a power-law behavior is found, from which we have obtained $\alpha_{MVI} = 0.383(8)$ for $p = 0$, $\alpha_{MVI} = 0.438(17)$ for $p = 0.005$, and $\alpha_{MVI} = 0.748(6)$ for $p = 0.025$.

From the values of α_{MVI} we can also obtain the exponents ν_{MVI} as we have made in Fig. 4 for the SVI. However, for $p = 0$ we have $\nu_{MVI} = 1.67 \pm 0.04$, which is far from the expected value for the standard percolation exponent $\nu_{SP} = 4/3$ [27]. In fact, we found that the exponent ν_{MVI} presents a maximum around $p = 0.001$ and decreases continuously until $p \sim 0.013$, where it reaches a value close to $\nu_{EW} = 0.35$, corresponding to the EW universality class (data not shown here).

We will see below that these poor results for ν_{MVI} can be understood by the spatial proximity of the other phase transitions. This is the main disadvantage of our method, which can generate spatial correlations between transitions separated by few lattice units leading to the occurrence of interference effects that hinder a more accurate determination of α_{MVI}, at least for the lattice sizes used in this paper.

C. Phase diagram

In order to locate the phase transitions showed in Figs. 2 and 4 and the percolation threshold, we have calculated the

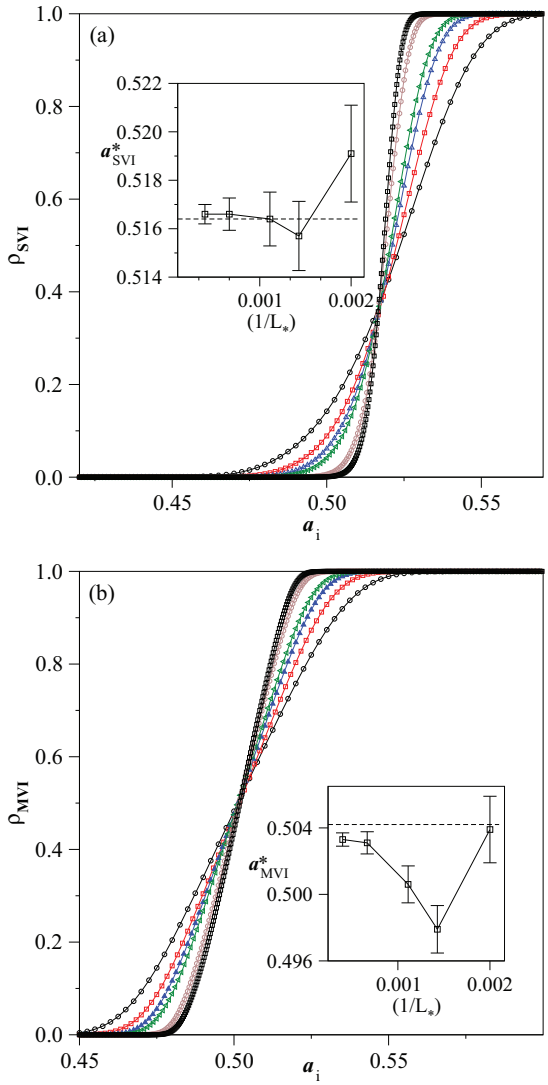

FIG. 5. (Color online) Clusters densities for the (a) SVI (ρ_{SVI}) and (b) MVI (ρ_{MVI}) as a function of the invasion parameter a for $p = 0.004$ and different lattice sizes. The insets show plots of the intersection points between different (but consecutive) curves against average values taken between consecutive gradients ($1/L_1$ and $1/L_2$), namely $1/L^* \equiv (1/L_1 + 1/L_2)/2$, which converges to $a_c = 0.5164 \pm 0.0006$ (a) and $a_{\text{perc}} = 0.5042 \pm 0.0006$ (b), represented by the dashed lines.

cluster density of the SVI (ρ_{SVI}) and MVI (ρ_{MVI}) for the phase B, as a function of the invasion parameter a with a gradient given by Eq. (2). These curves, for $p = 0.004$ and different lattice sizes, are shown in Figs. 5(a) and 5(b).

The intersection point of the cluster density for different gradients converges quickly to the transition point, as demonstrated in previous works [18–20]. On each inset of Figs. 5(a) and 5(b) the intersection point for consecutive gradients (or lattice sizes), a^*, is shown against the value of the mean gradient. The dashed horizontal line represents our estimated transition point, obtained from the linear fit of the intersection points. For $p = 0.004$ our estimated values are $a_c = 0.5164 \pm 0.0006$ and $a_{\text{perc}} = 0.5042 \pm 0.0006$, respectively. In the same way, we have obtained the critical points for the IPTs and

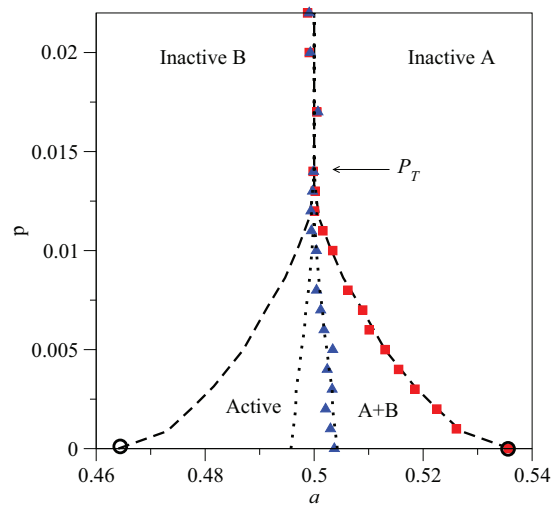

FIG. 6. (Color online) Phase diagram of the cyclic predator-prey model with neutral-pairs exchange p. The transition points (squares and circle), and percolation threshold (triangles) were obtained from the intersection point of the cluster density of the SVI (ρ_{SVI}) and MVI (ρ_{MVI}), respectively. P_T is the tricritical point with coordinates $p_T = 0.013 \pm 0.005$ and $a_T = 1/2$. For $p = 0$ the transition points are $a_A = 0.4644 \pm 0.0007$ and $a_B = 0.5356 \pm 0.0007$, and the percolation threshold are $a^A_{\text{perc}} = 0.4963 \pm 0.0027$ and $a^B_{\text{perc}} = 0.5037 \pm 0.0027$. Guides to the eyes: the dashed lines represent the first-order transition [$a_c(p)$] and the dotted lines represent the percolation threshold [$a_{\text{perc}}(p)$].

the threshold percolation using the SVI and MVI interfaces respectively, for several values of p. These results are drawn in the plane (a, p) of the Fig. 6. Note that Monte Carlo calculations were made just for B phase. However, by the symmetry of the model, we can draw the complete phase diagram of the system. The critical points for the A (a^A_c) phase are obtained from critical points of the B phase (a^B_c) by means of $a^A_c = 1 - a^B_c$.

We have indicated in Fig. 6 the active AB region as the phase where the A and B species are present, and the inactive A and B phases as the absorbing phases composed only by A and B species, respectively. We note that the reactive region shrinks since $p = 0$ until it disappears for a value identified as $p = P_T$. For $p > P_T$, our data show that the two transitions coincide. From a careful inspection of data in Fig. 6, the critical neutral-pair exchange is identified as $P_T = 0.013 \pm 0.005$, and because of the symmetry, it has horizontal coordinate given by $a_T = 1/2$.

From Figs. 4 and 6 we can see that the model presents three different critical behaviors: (i) for the line $p = 0$; (ii) for the region given by $0 < p < P_T$; and (iii) for the region $p > P_T$. We will analyze each of these behaviors.

(i) First of all, we can note from Fig. 6 that the reactive window (active $A + B$) presents its maximum extension for $p = 0$. Our estimate of the critical points for $p = 0$ [schematically represented in Fig. 1(a) as a_A and a_B] have been obtained as $a_A = 0.4644 \pm 0.0007$ and $a_B = 0.5356 \pm 0.0007$, whose values are in a good agreement with the previous results of Szabò and Szolnoki [17], who have found $a_A = 0.4666 \pm 0.0001$ and $a_B = 0.5358 \pm 0.0001$. Besides, from Fig. 4, we have shown that the exponent ν_{SVI} for $p = 0$

is compatible with the expected value for a second-order IPT belonging to the directed percolation universality class, again in agreement with the previous determination of Szabò and Szolnoki [17].

(ii) In Fig. 6 we observe that from the critical points a_A and a_B emerge two symmetric lines. In the region $0 < p < P_T$, these critical lines separate the active $A + B$ phase and the inactive A and B phases, and then those merge in the point P_T. As it was just observed, according to Fig. 4, for this region our method generated an interface whose exponent ν_{SVI} is compatible with the KPZ universality class. Then, we assume that these two lines correspond to a first-order IPTs. We recall that the first-order phase transition present in the Ziff-Gulari-Barshad model [28] (ZGB) also presents an interface in the KPZ universality class [18].

(iii) Finally, for $p > P_T$, as we can see from Fig. 6, the model presents a transition line between two inactive phases. Again, from Fig. 4, our method shows in this region an exponent ν_{SVI} compatible with ν_{EW}. We assume that these lines correspond to a first-order IPT, whose interface's behavior is given by the EW universality class. A similar behavior is presented by the monomer-monomer reaction model with attraction between different monomers whose interface has been found in the EW universality class [29].

It is worth noting that the change in the universality class of the first-order interface (from KPZ to EW) is due to the change on the nature of the phase transition. That is, for $0 < p < p_T$ it is a transition between an active phase and an absorbing phase, whereas for $p > P_T$, it is a transition between two absorbing and symmetric phases. Besides, despite the similarity of the results from the GM (see Fig. 3), these two transitions are quite different. For the latter case there is no active stationary states, since any finite system always reaches one of the two symmetric poisoned states. In this case, the critical point must be characterized by means of the dynamic behavior given by the temporal evolution of the observables going to the poisoned state, an outcome that is beyond the goal of this paper. This kind of transition is well known and has been extensively studied before, being the most important realization the monomer-monomer reaction model [30–32].

By noting that in the point P_T three lines of first order join, we have decided to call it "triple point". Also, comparing the Fig. 1 with our phase diagram (Fig. 6) we realize that the point p_c, showed in Fig. 1(b), is actually the triple point of our phase diagram of Fig. 6. Indeed, the value reported by Szabò and Szolnoki as $p_c = 0.01331(1)$ [13] is in excellent agreement with our determination.

From Fig. 6 we can see a pair of symmetric percolation threshold lines for $0 \leqslant p < P_T$: one of them between the percolating A phase and the nonpercolating A phase [the line at the left-hand side, here identified as $a^A_{MVI}(p)$], and the other one between the nonpercolating B phase and the percolating B phase [the line at the right-hand side, here identified as $a^B_{MVI}(p)$]. Also, comparing the location of the MVI and SVI in Fig. 6 we can see that for $0 \leqslant p < P_T$, the percolation transition occurs always into the reactive region. At the triple point P_T the percolation transition line joins with the first-order transition lines and, for $p \geqslant P_T$, the percolation transition and the first-order IPT coincide. In this way, for $p \geqslant P_T$ the percolating A (B) phase and the inactive A (B) phase coincides, and the nonpercolating A (B) phase is exactly the inactive B (A) phase. Therefore, beyond the triple point the transition between the inactive A and B phases is also a first-order percolation transition, as already found in the ZGB model [18,20] and in a variant of the Schlögl's second model under a gradient constraint [33]. We recall that, in order to have a first-order percolation transition from one first-order IPT, the latter should present a massive jump in the density of the majority species, at the transition point. Thus, if the jump at the density in the IPT is large enough, the poor phase does not percolate, while the rich one does, and consequently the percolation remains trapped in the jump and becomes of first order. In the present model, for $p \geqslant P_T$, this result is straightforward, since the jump at the critical point is maximum, that is from $\rho_B = 0$ (for $a < 1/2$) to $\rho_B = 1$ (for $a > 1/2$), and analogously for ρ_A. Because of that, in the phase diagram (Fig. 6) the critical lines $a_c(p)$ and $a_{\text{perc}}(p)$ coincide for $p \geqslant P_T$.

On other hand, below the triple point ($p < P_T$), both the critical lines $a_{SVI}(p)$ and $a_{MVI}(p)$ (see Fig. 6), and its characteristic exponents ν_{SVI} and ν_{MVI}, are different. For this case, at the transition point, the system moves from the active phase, with high density of ρ_B, to the inactive B, with density $\rho_B = 1$ (analogously for ρ_A). Despite that we have a first-order IPT, the jump in the density is not enough to trap the percolation transition. So the percolation transition lies at the active region, as can be seen from Fig. 6.

Also, from Fig. 6, we can observe that the two percolation transition lines [$a^A_{MVI}(p)$ and $a^B_{MVI}(p)$] are very close. For $p = 0$ their distance is about 0.007 and at the triple point they joint each other. The poor values obtained in the previous section for the exponent α_{MVI} can be explained for the closeness of the two percolation transition lines, since from Fig. 3(b) we have that $w_{MVI} \sim 0.01$ and the two MVI interfaces are certainly interfering. This artifact could be avoided using smaller gradients in order to make the distance between the transition percolation lines greater than the width of the MVI interface. That is, the following condition should be valid

$$w_{MVI} \ll \left|a^B_{MVI}(p) - a^A_{MVI}(p)\right|. \tag{7}$$

Anyway, the necessary lattice size to obey this condition in the present model becomes prohibitive, particularly for values close to P_T.

Figure 6 shows that also the presence of the first-order IPT can hinder a more accurate determination of α_{MVI}, mainly near the triple point P_T. In fact this effect was previously observed for the ZGB [19], where nearby first-order transition is present. On the other hand, when there are no nearby IPTs in the model, one can evaluate the exponent α_{MVI} accurately [18–20,33].

It is important to note that Fig. 6 represents the complete p versus a phase diagram of the system.

V. STANDARD SIMULATIONS

In order to compare and detect the differences in the behavior of the first- and the second-order IPTs, we have also performed extensive standard simulations for two values of p, i.e., $p = 0$ and $p = 0.004$. Here the algorithm is the same as we have used with the GM (described in Sec. II), with the only

difference that the invasion probability a is kept constant over all the lattice at one fixed value.

Usually the simulation techniques for second- and first-order transition are quite different. That is because first-order transitions methods intend to avoid metastability and to understand the hysteretic effects, whereas second-order transitions methods intend to manage the critical slowing down [34].

In the case of the first-order IPTs to absorbing states, one of the simplest and most established methods to estimate the critical point involves the calculation of the probability of reaching the absorbing state [28]. In order to avoid metastabilities, the initial conditions are chosen as half of the lattice being in the absorbing phase and the other one being in the active phase. Then, at the end of a simulation run, the probability $P_{\text{abs}}(a)$ of the system to reach the absorbing state is calculated for a given value of the control parameter a. To obtain confident estimated values, this prescription must be performed a large number of times for each lattice size. Also the simulation time must be long enough to ensure that the final results do not depend on the length of the simulation. Recently, it has been shown that $P_{\text{abs}}(a)$ is a sigmoid function from which it is possible to estimate the characteristic values of a first-order IPTs [35]. Thus, the location of the transition point (a_c) is taken as the point where the probability of reaching the absorbing state is equal to the probability of reaching the active phase [that is $P_{\text{abs}}(a_c) = 1/2$] [28]. We refer to this method to estimate a_c as the equal probability criteria.

Since a_c depends on the lattice size, we must take into account finite-size effects. In the theory of first-order equilibrium transition it has been shown that defining one effective size-dependent critical point (for example with the peak of the susceptibility) we can extrapolate the thermodynamical value by means of following rule

$$a_c(L) = a_c(L \to \infty) + AL^{-D}, \tag{8}$$

where A is a constant and D is the dimensionality of the system [34]. However, this relationship has been shown to be valid, also for first order IPT transitions [28,35].

In order to implement this method here, the initial configuration is obtained by filling randomly a half of the lattice with the four species and the other half with only B species. Also, the lattice size ranges from $L = 75$ to $L = 800$, the total simulation time considered is $t_s = 4 \times 10^5$, and the number of samples is $n = 200$ for smaller lattices and $n = 100$ for the largest ones.

Figure 7 shows the estimated critical point $a_c(L)$ for $p = 0.004$ by using the equal probability criteria. Here we plot the critical point a_c against L^{-D}, with $D = 2$, so that the straight line is a fit of the data according to Eq. (8). We can observe a very good agreement with the proposed power law for $L \geqslant 100$. The critical point at the thermodynamic limit [$a_c(L \to \infty)$], obtained from the extrapolation given by Eq. (8), is $a_c = 0.5159(1)$. This value is fully consistent with that one obtained from the GM, that is $a_c = 0.5164 \pm 0.0006$. It should be stressed that the results of Fig. 7 constitutes an additional confirmation that the IPT for $p = 0.004$ is a first-order transition, in agreement with the results showed in Fig. 6 obtained with the GM method.

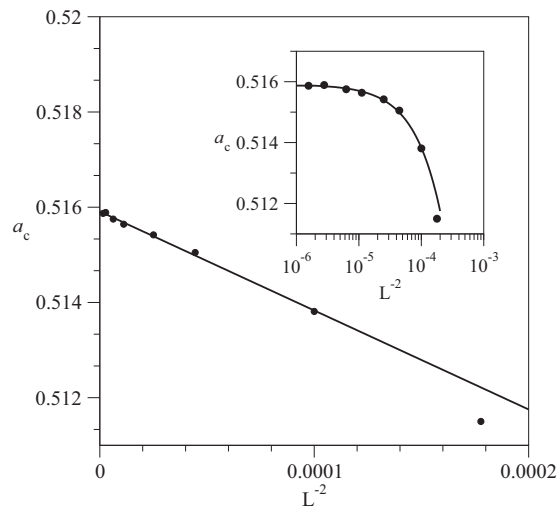

FIG. 7. Standard simulation results for the first-order phase transition at $p = 0.004$: critical point a_c, obtained from the equal probability criteria, as a function of L^{-D}, with $D = 2$. The straight line is a fit of the data by using the finite-size theory according to Eq. (8). Inset shows a linear-log plot of the data. The obtained extrapolated value [$a_c(L \to \infty)$] is $a_c = 0.5159(1)$.

In order to compare the behaviors of the first- and second-order IPTs, we have also performed similar standard simulations for the case where the exchange probability is absent ($p = 0$). Employing the same set of parameters and initial conditions as in the previous case, we have determined the probability of the system to reach the absorbing state for a given value of the control parameter a [$P_{\text{abs}}(a)$].

For the continuous transitions the finite-size critical points are governed by the correlation length exponent ν. In this way, the equivalent of Eq. (8), is given by

$$a_c(L) = a_c(L \to \infty) + CL^{-1/\nu}, \tag{9}$$

where C is a constant. This power law is usually applied to estimate both critical points in equilibrium phase transitions [34] and percolation thresholds in percolative transitions [27]. Here, we propose to use Eq. (9) in second-order IPTs with the finite-size estimate for the transition points given by the equal probability criteria.

Figure 8 shows these estimated $a_c(L)$ against $L^{-1/\nu}$, with $\nu = \nu_{DP} = 0.733$, the value of the correlation length exponent for the DP universality class [25]. The straight line is a fit of the data according to Eq. (9). Our extrapolated value for the critical point is $a_c = 0.5359(1)$, which is fully consistent with the estimated obtained by means of the GM for $p = 0$, that is $a_c = 0.5356 \pm 0.0007$. Also both values are in agreement with those obtained previously by Szabò and Szolnoki [17], $a_c = 0.5358 \pm 0.0001$.

In this way, following the results from long standard simulations for $p = 0$, the critical behavior of the system is correctly governed by the DP exponent $\nu_{DP} = 0.733$. In contrast, for the same kind of simulations for $p = 0.004$, the relevant exponent is the dimensionality $D = 2$, as expected for a first-order transition. We remark that these results are consistent with the phase diagram shown in the Fig. 6 and

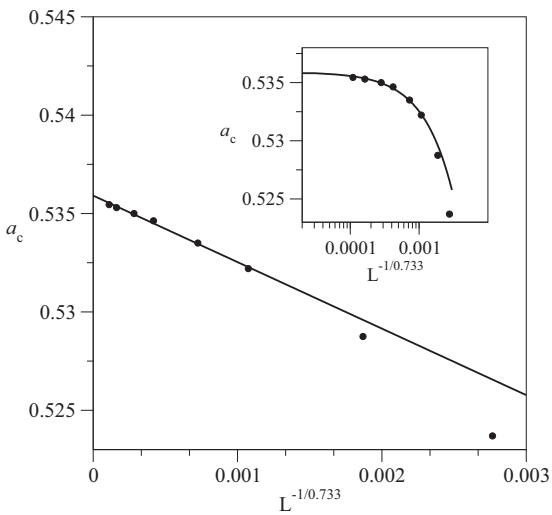

FIG. 8. Standard simulation results for the continuous phase transition at $p = 0$: critical point a_c, obtained from the equal probability criteria, as a function of $L^{-1/\nu}$ with $\nu_{DP} = 0.733$ [25]. The straight line is a fit of the data by using the finite-size theory according to Eq. (9). The obtained extrapolated value $[a_c(L \to \infty)]$ is $a_c = 0.5359(1)$.

with the discussions and results obtained in the preceding sections.

VI. CONCLUSIONS

In the present work we have studied a four-species cyclic predator-prey lattice model by using the gradient method and standard simulations. We have obtained the phase diagram using as relevant parameters the invasion rate a of prey sites by neighboring predators, and the exchange probability p, by which noninteracting species can exchange their positions. Previous results for $p = 0$ and $a = 1/2$ are recovered and included here. By changing these parameters the model can present an active phase (where the four species invade each other cyclically) and two symmetric absorbing phases composed by only two noninteracting species (neutral pairs).

In the absence of the exchange between neighboring neutral pairs ($p = 0$) our results show the presence of two symmetric continuous transitions: one between the active phase and the absorbing A phase ($a_A = 0.4644 \pm 0.0007$) and other one between the active phase and the absorbing B phase ($a_B = 0.5356 \pm 0.0007$), in agreement with Ref. [17]. The critical behavior of these points in both the gradient method and standard simulations is dominated by the direct percolation length correlation exponent, as expected for a continuous phase transition in the DP universality class ($\nu = 0.733$) also in agreement with previous studies [17].

When a non-null exchange probability p, between neighboring neutral pairs, is considered the two continuous critical points present for $p = 0$ become two transition lines between the active $A + B$ phase and the absorbing A (B) phase (A for $a < 1/2$ or B for $a > 1/2$). By increasing the exchange p the reactive window, limited by these two transition lines, shrinks and finishes in a triple point P_T.

We argue that the exchange probability p changes the order of the phase transitions, which becomes first order for $p > 0$. This effect is shown by means of the gradient method, which detects an interface in this region compatible with the KPZ universality class. Also, it is verified by means of standard simulations (for $p = 0.004$) that the estimated transition point obtained by the equal probability criteria, converges to the thermodynamical one governed by the dimensionality $D = 2$, as expected for a first-order transition. In contrast, for $p > P_T$, we observe a first-order line transition, with $a = 1/2$, between two symmetric absorbing states with a zero-wide reactive window. For this region the interface generated by the gradient method shows a scaling behavior compatible with the EW universality class. We recall that the change in the universality class of the first-order interface (from KPZ to EW) is due to the change on the nature of the phase transition. In fact, for $0 < p < p_T$ the model presents a transition between an active phase and an absorbing phase, whereas for $p > P_T$, it has a transition between two absorbing phases. The behavior of these first-order transition lines are qualitatively similar to that for the monomer-monomer reaction model with repulsive interaction between the two different species. In the simplest monomer-monomer model there is a reactive window of zero width [29] and the interface, formed between solid domains of each species, is in the KPZ universality class. However when repulsive interactions acts, the interface has been associated to the EW universality class [29]. We can argue that the repulsion between different species in the monomer-monomer model, causes the same effect that high values of the probability of the interchange between neutral species in our model, that is a smoother interface in the EW universality class.

One relevant point in the phase diagram is the *locus* where the three lines of transition join (P_T). We have estimated the coordinates for this triple point as $P_T = 0.013 \pm 0.005$ with $a_T = 1/2$. Szabó *et al.* have previously described this point as a transition between an active phase and one of two possible symmetric absorbing phases, and have estimated it as been $p_c = 0.01331(1)$ [16]. Here we have shown that this symmetry breaking point is actually a triple point, which plays an important role in the first-order IPTs, since it separates two different kinds of first-order IPTs with different interface behavior.

Additionally, we have determined the percolation transition, and again, the triple point plays a central role (see Fig. 1). In fact, it separates a standard-percolation line in the SP universality class (for $p < P_T$), within the active $A + B$ phase, from a first-order percolation line (for $p > P_T$) that coincides with the A-B first-order IPT.

ACKNOWLEDGMENTS

The authors would like to acknowledge the Brazilian Science Agency CNPq (475039/2010-6), the Argentinian Science Agencies CONICET and ANPCyT, Universidade Federal de Santa Catarina (UFSC) and Universidad Nacional de La Plata (UNLP) for the financial support. We thank Ezequiel V. Albano for his critical reading of the present work.

[1] L. L. Jiang, T. Zhou, M. Perc, and B. H. Wang, Phys. Rev. E **84**, 021912 (2011).
[2] T. Reichenbach, M. Mobilia, and E. Frey, Phys. Rev. Lett. **99**, 238105 (2007).
[3] *Evolutionary Games and Population Dynamics*, edited by J. Hofbauer and K. Sigmund (Cambridge University Press, Cambridge, 1998).
[4] G. Szabó and G. Fáth, Phys. Rep. **446**, 97 (2007).
[5] R. A. Lankau, E. Wheeler, A. E. Bennett, and S. Y. Strauss, J. Ecol. **99**, 176 (2011).
[6] B. Sinervo and C. M. Lively, Nature (London) **380**, 240 (1996).
[7] B. Kerr, M. A. Riley, M. W. Feldman, and B. J. M. Bohannan, Nature (London) **418**, 171 (2002).
[8] B. C. Kirkup and M. A. Riley, Nature (London) **428**, 412 (2004).
[9] J. E. Satulovsky and T. Tomé, Phys. Rev. E **49**, 5073 (1994).
[10] T. Tomé and R. M. Ziff, Phys. Rev. E **82**, 051921 (2010).
[11] B. Drossel and F. Schwabl, Physica A **199**, 183 (1993).
[12] P. Bak, K. Chen, and C. Tang, Phys. Lett. A **147**, 297 (1990).
[13] G. Szabó, A. Szolnoki, and G. A. Sznaider, Phys. Rev. E **76**, 051921 (2007).
[14] A. F. Lütz, S. Risau-Gusman, and J. J. Arenzon, J. Theor. Biol. **317**, 286 (2013).
[15] K. Sato, N. Yoshida, and N. Konno, Appl. Math. Comp. **126**, 255 (2002).
[16] G. Szabó, J. Phys. A **38**, 6689 (2005).
[17] G. Szabó and A. Szolnoki, Phys. Rev. E **77**, 011906 (2008).
[18] N. Guisoni, E. S. Loscar, and E. V. Albano, Phys. Rev. E **83**, 011125 (2011).
[19] E. S. Loscar, N. Guisoni, and E. V. Albano, Phys. Rev. E **80**, 051123 (2009).
[20] E. S. Loscar, N. Guisoni, and E. V. Albano, Eur. Phys. J. B **85**, 60 (2012).
[21] B. Sapoval, M. Rosso, and J. F. Gouyet, J. Phys. Lett. **46**, L149 (1985).
[22] V. C. Chappa and E. V. Albano, J. Chem. Phys. **121**, 328 (2004).
[23] F. D. A. Aarão Reis, Phys. Rev. E **63**, 056116 (2001).
[24] *Non-equilibrium Phase Transitions and Critical Phenomena, Vol. I, Absorbing Phase Transitions*, edited by M. Henkel, H. Hinrichsen, and S. Lubeck (Springer, Bristol, 2008).
[25] *Nonequilibrium Phase Transitions and Critical Phenomena*, edited by J. Marro and R. Dickman (Cambridge University Press, Cambridge, 1999).
[26] *Fractal Concepts in Surface Growth*, edited by A. L. Barabasi and H. E. Stanley (Cambridge University Press, Cambridge, 1995).
[27] *Introduction to the Percolation Theory*, edited by D. Stauffer and A. Aharoni (Taylor & Francis, London, 1992).
[28] R. M. Ziff, E. Gulari, and Y. Barshad, Phys. Rev. Lett. **56**, 2553 (1986).
[29] H. C. Kang and W. H. Weinberg, Phys. Rev. E **47**, 1604 (1993).
[30] J. W. Evans and T. R. Ray, Phys. Rev. E **47**, 1018 (1993).
[31] M. A. Sanservino, A. Lopez, E. V. Albano, and R. A. Monetti, Eur. Phys. J. B **40**, 305 (2004).
[32] E. V. Albano, Heterogen. Chem. Rev. **3**, 389 (1996).
[33] M. T. Gastner, B. Oborny, A. B. Ryabov, and B. Blasius, Phys. Rev. Lett. **106**, 128103 (2011).
[34] *A Guide to Monte Carlo Simulations in Statistical Physics*, edited by D. P. Landau and K. Binder (Cambridge University Press, Cambridge, 2005).
[35] I. Sinha and A. K. Mukherjee, J. Stat. Phys. **147**, 707 (2012).